Journal of Power Sources 195 (2010) 1007–1014

Contents lists available at ScienceDirect

Journal of Power Sources

journal homepage: www.elsevier.com/locate/jpowsour

Influence of operating temperature on cell performance and endurance of high temperature proton exchange membrane fuel cells

Yuka Oono [a], Takashi Fukuda [a], Atsuo Sounai [b], Michio Hori [a,*]

[a] Fuel Cell Research Center, Daido University, 10-3 Takiharu-cho, Minami-ku, Nagoya, Aichi 457-8530, Japan
[b] Dept. of Materials Science & Engineering, Suzuka National College of Technology, Shirako-cho, Suzuka, Mie 510-0294, Japan

ARTICLE INFO

Article history:
Received 11 April 2009
Received in revised form 21 August 2009
Accepted 24 August 2009
Available online 15 September 2009

Keywords:
High temperature proton exchange membrane fuel cells
Performance
Durability
Polybenzimidazole
Phosphoric acid
Deterioration

ABSTRACT

The relation between high temperature proton exchange membrane fuel cell (HT-PEMFC) operation temperature and cell durability was investigated in terms of the deterioration mechanism. Long-term durability tests were conducted at operational temperatures of 150, 170, and 190 °C for a HT-PEMFC with phosphoric acid-doped polybenzimidazole electrolyte membranes. Higher cell temperatures were found to result in a higher cell voltage, but decrease cell life. The reduction in cell voltage of approximately 20 mV during the long-term tests was considered to be caused both by aggregation of the electrode catalyst particles in the early stage of power generation, in addition to the effects of crossover due to the depletion of phosphoric acid in the terminal stage, which occurs regardless of cell temperature. It is expected that enhanced long-term durability for practical applications can be achieved through effective management of phosphoric acid transfer.

1. Introduction

Fuel cells have attracted considerable attention as an environmentally friendly, clean energy system and a broad range of research has been conducted in this area. Presently, the most actively studied fuel cell is the perfluorosulfonic acid-type low temperature proton exchange membrane fuel cell (LT-PEMFC). The LT-PEMFC is different from previous generation fuel cells in that it uses a solid polymer membrane as the electrolyte, so that it conducts protons via water, and can therefore operate in the temperature range below 100 °C. Consequently, the LT-PEMFC has extended the range of applications of fuel cells to small-scale power sources for automobiles, portable and residential use, and this trend is expected to continue into the future. The recent trend in Japan is the commercialization of 1 kW-class domestic cogeneration systems using both electricity and electrically generated waste heat, due to significant improvements in fuel cell performance and durability [1]. However, a major stumbling block for commercialization is that the system tends to be very complex and expensive because LT-PEMFCs inherently require humidification for proton conduction via water. In addition, the system efficiency is relatively low due to the low operating temperature of <100 °C [1], and it requires a CO selective oxidizer as the CO resistance of the electrode catalyst is reduced at lower temperatures [2–5].

The development of next generation PEMFCs is actively being researched in order to solve these problems by simplification of the system, reduction of production costs, and improvement of the operational efficiency in the temperature range of 150–200 °C [6]. In addition, next generation PEMFCs must have sufficient heat resistance under zero humidification conditions, and be based on polymer electrolytic membranes that can chemically couple with acids capable of proton conduction. Research has been conducted on acids that are capable of proton conduction at temperatures exceeding 100 °C, in addition to various polymers that adsorb acids [7–12], and the results suggest that sulfuric and phosphoric acids have high proton conduction capability [13–15]. With regard to the polymers that form the structure of the membranes, various elementary studies have been carried out on polybenzimidazole (PBI) [16], polyethylene oxide (PEO) [17], polyvinyl alcohol (PVA) [18,19], polyacrylamide (PAAM) [20,21] and polyethylenimine (PEI) [22].

Further studies have focused on high temperature proton exchange membrane fuel cells (HT-PEMFCs) using PBI membranes doped with phosphoric acid as the electrolyte membrane, from the point of view of membrane conductivity and heat resistance [23–25], and the power generation of actual cells [26–34]. Zhang et al. reported that higher cell performance was achieved as the operating temperature approached 200 °C [6]. In addition, the results of long-term power generation tests (exceeding 10,000 h) have been

* Corresponding author. Tel.: +81 52 612 6111x2508; fax: +81 52 612 5623.
E-mail address: hori@daido-it.ac.jp (M. Hori).

0378-7753/$ – see front matter © 2009 Published by Elsevier B.V.
doi:10.1016/j.jpowsour.2009.08.097

reported by BASF and Samsung [35,2], and these PEMFCs are considered to be the closest to commercial viability.

However, there is a dilemma in that raising the operating temperature in order to increase the cell voltage and improve the efficiency makes it difficult to sustain long-term durability. Conversely lowering the temperature improves the durability but leads to lower cell voltages. To date, only a few reports have dealt with the relationship between the operating temperature and the cell durability, including the deterioration mechanism during approximately 500 h operation at 150 °C [28–31].

Therefore, in this study, the effects of temperature on the cell voltage and durability were evaluated by conducting long-term durability tests on cells using PBI membranes doped with phosphoric acid and using newly developed electrodes for cell temperatures of 150, 170, and 190 °C. The deterioration mechanism of the cells was investigated based on the results of time variations of cell voltage, internal cell resistance and impedance during the durability tests, in addition to post-analysis by transmission electron microscopy (TEM) observations.

2. Experimental

2.1. Preparation of PBI electrolyte membrane

PBI membranes (5.5 cm × 5.5 cm, ca. 40 μm thick) provided by the Joint Research Institute were immersed in a 85% phosphoric acid solution heated to 40 °C for 40 min to dope the membranes [36]. Identical membranes doped under identical conditions were used for all tests in this study. The phosphoric acid doping ratio was determined by measuring the weight of the membranes before and after doping using a precision electronic balance (AUW120D Shimadzu Corp., Japan). The doping ratio was defined as the weight of phosphoric acid doped into the membrane divided by the weight of the membrane after doping.

2.2. Production of electrodes

A sheet of carbon paper with a thickness of 280 μm (TGP-H-090, Toray Corp., Japan) was used as a gas diffusion layer. A mixed powder of Ketchen Black (EC-600JD, Akzo Nobel Corp., UK) and polytetrafluoroethylene (PTFE, DuPont) in a weight ratio of 65:35 was applied onto the carbon paper using a dry coating device [36–38] until it formed a coating of 2 mg cm^{-2}. This was then heated at 350 °C in an atmospheric oven, and the surface leveled by a roller press [36–38] to produce a filled carbon layer.

A catalyst ink was then prepared by mixing polyvinylidene fluoride (PVDF; Kureha Corp., Japan), Pt–Co-supported on Ketchen Black powder (carbon/metal: 50/50, TKK Corp., Japan) [36] and N-methyl pyrrolidone (NMP; Sigma–Aldrich Corp., USA) with agitation for 60 h. For preparation of the electrode, the catalyst ink was applied using a wet coating method onto the coated carbon paper, dried for 1 h at 80 °C in air, and then finally held in a vacuum oven at 160 °C for 25 h to remove NMP [36].

The amount of supported Pt was approximately 0.8 mg cm^{-2} for both anode and cathode electrodes.

2.3. Single cell assembly

The electrolyte membrane doped with phosphoric acid was sandwiched by two electrodes prepared according to Section 2.2 to produce the membrane electrode assembly (MEA). This was sandwiched between a pair of bi-polar plates made of carbon, on which a serpentine flow pattern was machined. The flow pattern was designed by Japan Automobile Research Institute (JARI) and had a reaction area of 5 cm × 5 cm. Further, this assembly was in turn sandwiched by current collector plates and stainless steel end plates fitted with a rubber heater on the outermost surface and tightened using eight M6 bolts to produce a single cell [36]. Five of these single cells were prepared.

2.4. Single cell power generation tests

The five single cells described in Section 2.3 were mounted on a fuel cell test stand (Kofloc Corp., Japan) equipped with mass-flow controllers, an electronic loading device (Kikusui Electronics Corp., Japan) for controlling the electric current, an AC milliohm tester (Model 3566, Tsuruga Electric Corp., Japan) with a constant frequency of 1 kHz, and a personal computer for equipment monitoring and data output. Tests of the initial characteristics, long-term durability and power output over 1000 h were conducted on a single cell, three single cells and the remaining single cell, respectively. During all tests, 130 mL min^{-1} (stoich: 3.7) of pure hydrogen was supplied to the anode side, and 310 mL min^{-1} (stoich: 3.7) of air or 66 mL min^{-1} (stoich: 3.7) of pure oxygen was supplied to the cathode side, with none of the reaction gases being humidified [36]. All power generation processes were conducted under atmospheric conditions.

2.4.1. Initial performance test

In this test, power was generated from a single cell at a cell temperature of 150 °C and a current density of 0.2 A cm^{-2} for 500 h until the cell voltage reached its peak and stabilized. The cell temperature was then varied from 120 to 200 °C with 10 °C increments, holding the temperature at each stage for approximately 1 h to measure the cell voltage and internal resistance.

The impedance was then measured by sweeping a constant AC current of 5 A (0.2 A cm^{-2}) with an amplitude of 0.5 A within the frequency range of 20,000–0.01 Hz using a potentiostat–galvanostat (HZ 5000 HAG-3001, Hokuto Denko Corp.) and a frequency response analyzer (FRA 5020A, NF Corp., Japan) to examine details of the cell resistance [36]. In this case, hydrogen was supplied to the anode side and pure oxygen to the cathode side.

2.4.2. Long-term durability test

In this test, the temperatures of the three single cells were fixed at 150, 170, and 190 °C, respectively, and the current density was controlled to maintain a current density of 0.2 A cm^{-2} using an electronic loading device. In this case, the rate of decrease in cell voltage was calculated based on the difference between the peak cell voltage and that measured during long-term power generation. Power generation was terminated when the cell voltage dropped by 10%. For the cell at 170 °C, the impedance was measured in the same manner as described in Section 2.4.1 after 5000 h of operation, and power generation was then terminated.

The remaining cell was operated for approximately 1000 h at 150 °C at a current density of 0.2 A cm^{-2} and the catalyst was then examined using TEM.

2.5. Post-analysis

TEM observations were carried out both on as-prepared electrode catalysts and those following testing for about 1000 h at 150 and 190 °C. In addition, scanning electron microscopy (SEM) observations were performed on the membrane subjected to the long-term durability test at 170 °C.

3. Results and discussion

3.1. Initial performance test

Fig. 1 shows the relation between the cell voltage and cell temperature obtained from the initial performance test described in

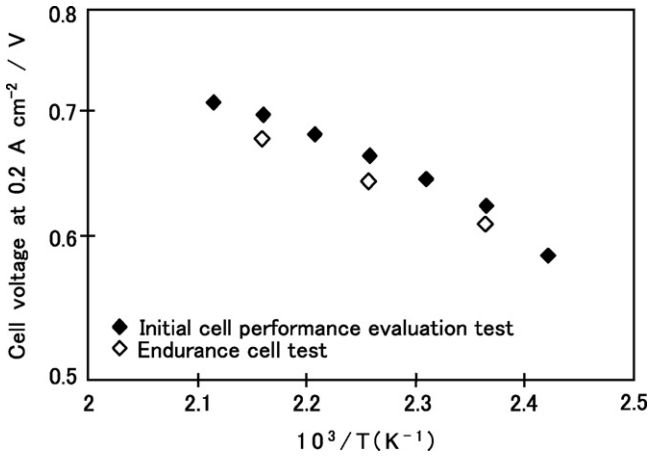

Fig. 1. Relationship between cell voltage and cell temperature obtained from the power generation tests.

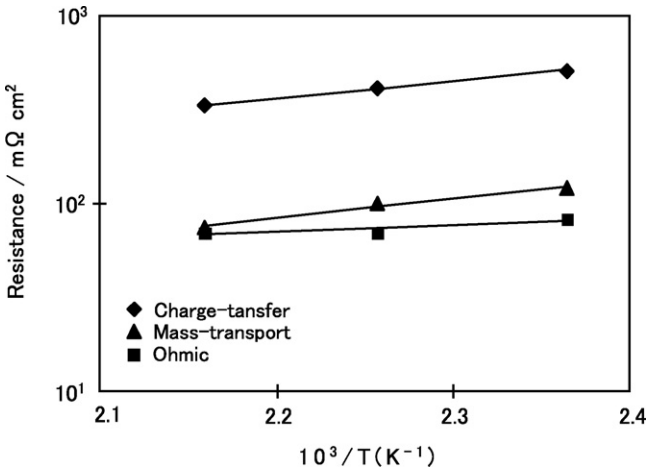

Fig. 3. Relationship of the ohmic, charge transfer and mass transport resistance to the cell temperature.

Section 2.4.1. As can be seen, the cell voltage increased by approximately 100 mV when the cell temperature was raised from 120 to 140 °C. When the cell temperature was subsequently raised from 140 to 200 °C in increments of 10 °C, the cell voltage increased at a rate of approximately 10 mV per 10 °C, i.e., at 1 mV °C^{-1}. A similar dependence of cell voltage on temperature has been previously reported for phosphoric acid-PBI electrolyte membranes [6,26,27].

Fig. 2 shows a Cole–Cole plot obtained from impedance measurements conducted at 0.2 A cm^{-2} for the same single cell, whereas Fig. 3 plots the ohmic, electric charge transfer, and mass transport resistance values derived from the data of Fig. 2 relative to the cell temperatures.

As can be seen, the ohmic resistance drops slightly with increasing cell temperature. In general, ohmic resistance is related to electrical resistance, contact resistance, and the membrane proton conductivity. The decrease in ohmic resistance seen in Fig. 3 is believed to be due to an improvement in proton conductivity in the electrolyte membrane with increasing cell temperature. This is supported by the work of Zhang et al. [6] on the influence of cell temperature on membrane resistance, and the relation between proton conductivity in phosphoric acid-PBI electrolytic membranes and cell temperature reported by Ma et al. [24].

Furthermore, Fig. 3 shows that the charge transfer resistance is markedly reduced with increasing cell temperature. It is generally believed that the electrical charge transfer resistance is related to the catalyst activity of the cathode and anode. Therefore, it seems likely that an increase in temperature gave rise to an increase in catalyst activity, promoting electrode reactions and consequently leading to an increase in cell voltage. Zhang et al. also measured the impedance spectra of HT-PEMFCs at various cell temperatures and similarly concluded that the charge transfer resistance is reduced by the promotion of anode oxidization and cathode reduction as the cell temperature increases [6]. Further, Ajani et al. showed that the activation overpotential of HT-PEMFCs was reduced as the cell temperature increased [26], which lends further support to this idea.

In Fig. 3, it can be seen that a slight reduction in the mass transport resistance occurs as the cell temperature increases. The mass transport resistance is determined by the rate of diffusion of the reactant gas in the porous electrode and the electrolyte, and by its solubility into the electrolyte. Increasing the cell temperature leads not only to higher gas diffusion rates, but also a reduction in gas solubility. Which of these factors has the dominant influence on the mass transport resistance depends on the current density. It has been reported that at high current density, the reduction in gas solubility dominates and an increase in cell temperature leads to a higher mass transport resistance [6]. However, in this study, the impedance measurements were conducted at a low current density of 0.2 A cm^{-2}. Under these conditions, the enhancement of gas diffusion had the largest impact, leading to a reduction in mass transport resistance as the temperature increased.

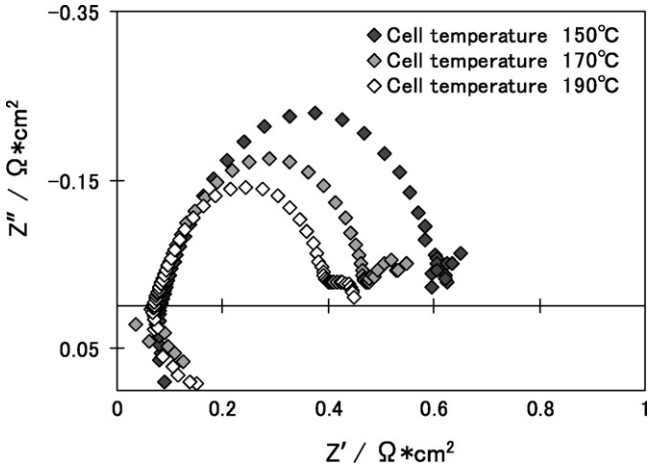

Fig. 2. Cell temperature dependence of the Cole–Cole plots at 0.2 A cm^{-2} for an initial performance evaluation after 500 h operation.

3.2. Long-term durability test

Fig. 4(a), (b), and (c) shows the changes in cell voltage and internal resistance over time during the long-term durability tests at 150, 170, and 190 °C, respectively. In these tests the current density was constant at 0.2 A cm^{-2}.

As seen in Fig. 4(a), in the case of the 150 °C cell, the cell voltage gradually increased from the beginning of power generation, reached a peak value after several hundred hours, and then declined very gradually for the remaining period. Even following 16,000 h (2 years) of operation, the cell voltage is still within 7% of its peak value, and the power generation test is currently still in progress. The three temporary drops which appear in the curve are due to emergency stops of the test stand. On the way, up to approximately 12,000 h, no significant changes were observed in the cell internal resistance, which is related to the ohmic resistance and the proton conductivity resistance, although a gradual increase was observed over 12,000 h.

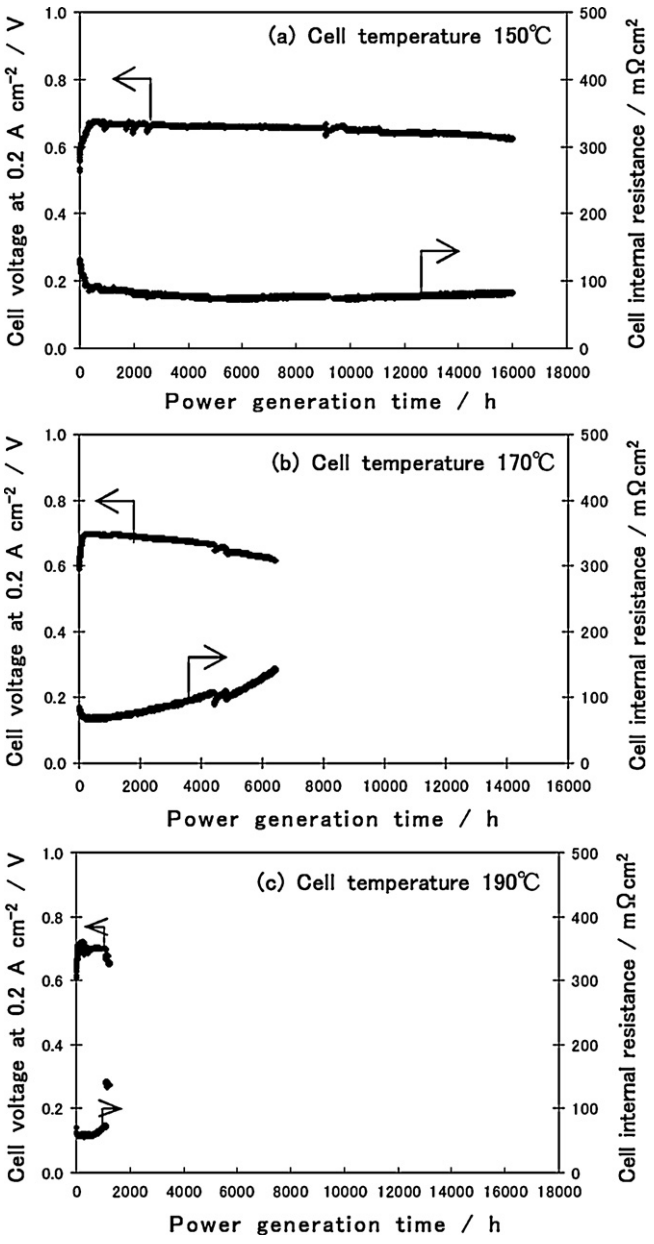

Fig. 4. Time course of cell voltages and internal resistances of three cells operated at 0.2 A cm^{-2} at cell temperatures of 150, 170, and 190 °C.

In the 170 °C cell shown in Fig. 4(b), the cell voltage increased relatively rapidly from the beginning of power generation, reached its peak value in a few hundred hours, and then dropped gradually. At around 4500 h, a sharp drop occurred due to a gas stoppage incident, but recovery took place within several hundred hours. However, from approximately 5000 h, the cell voltage began to drop with increasing speed. Power generation was terminated after 6400 h of operation, at which point the cell voltage had declined 10% from its peak value. During the entire duration of the test, apart from the very early period, the internal resistance continued to increase as the voltage decreased.

As seen in Fig. 4(c), the voltage of the 190 °C cell reached a peak almost immediately after the start of the power generation and then dropped due to a gas stoppage incident, similar to those for the 150 and 170 °C cells. However, in contrast to the other two cells, the cell voltage did not quickly recover, but remained at a low level for approximately 500 h, and then dropped sharply after

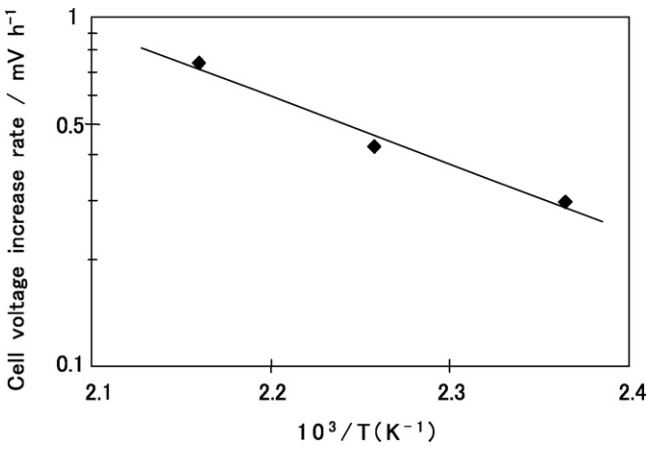

Fig. 5. Relationship of cell voltage increase rate to cell temperature during initial power generation.

1000 h of operation. Power generation was terminated after 1220 h of operation when the cell voltage had dropped by 10% from its peak value.

Fig. 5 shows the relation between the rate of increase of the cell voltage during the initial period of power generation and the cell temperature, which was obtained by arranging the results shown in Fig. 4. Clearly, the initial cell voltages increase more rapidly as the temperature increases. The initial time required for the cell voltage to stabilize is considered to correspond to the time taken for the NMP solvent remaining in the catalyst layer to evaporate and for the space thus produced to be filled with enough phosphoric acid to secure a sufficient charge transfer path in the cell [37]. In fact, all of the cell temperatures are fairly close to the boiling point, 220 °C, of NMP. In particular, in the cell operating at 190 °C, the solvent would be expected to quickly evaporate due to its high saturated vapor pressure.

Fig. 6 shows the rate of decrease of the cell voltage from its peak value as a function of the cell temperature. For the 150 °C cell, the rate was obtained by dividing the cell voltage drop from its peak to 16,000 h, read from Fig. 4(a), by the power generation time of 16,000 h. For the 170 and 190 °C cells, the rates were obtained by dividing the cell voltage drops of 10% from the peak voltage, shown in Fig. 4(b) and (c), by the final power generation time of 6400 and 1220 h, respectively. As seen in Fig. 6, the cell voltage deterioration rate was strongly dependent on temperature, and had a value of 3.6 μV h^{-1} for a cell temperature of 150 °C.

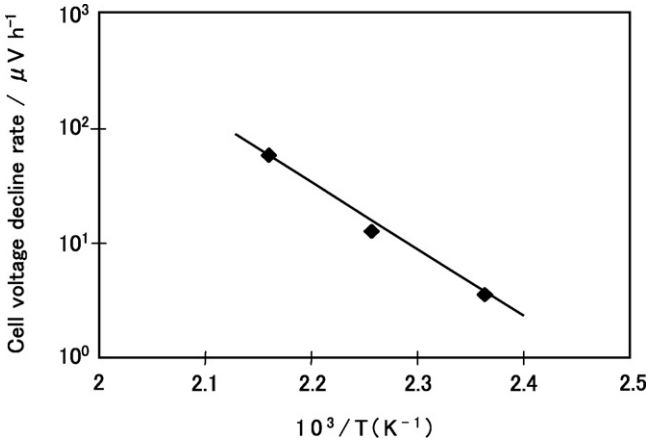

Fig. 6. Relationship of cell voltage decline rate to cell temperature over long-term power generation.

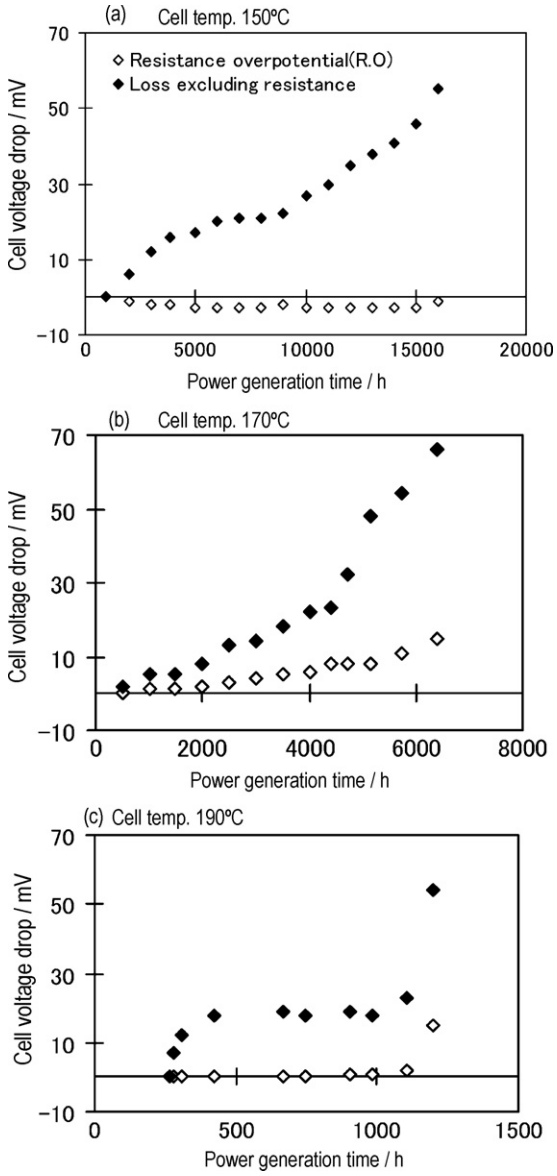

Fig. 7. Time course of the cell voltage drop due to the resistance overpotential and losses except cell resistance for cells operated at 150, 170 and 190 °C.

Fig. 7 shows the time dependence of the resistance overpotential and the cell voltage loss excluding resistance. The "resistance overpotential" is the product of the current density (0.2 A cm^{-2}) and the cell internal resistance taken from Fig. 4. "Loss excluding resistance" is obtained by subtracting the resistance overpotential portion from the total cell voltage drop. Therefore, the loss excluding resistance includes the increase of activation overpotential, the increase of diffusion overpotential, and the decrease in the open circuit voltage (OCV). However, the effect of diffusion overpotential is very small, because the long-term durability tests were conducted at a low current density of 0.2 A cm^{-2}, as has been discussed previously.

As shown in Fig. 7(a), for the cell operating at 150 °C, the resistance overpotential dropped gradually from the initial period of power generation to approximately 4000 h, and remained constant thereafter until 16,000 h. On the other hand, the loss excluding resistance increased gradually from approximately 500 h, became almost constant from about 5000 to 10,000 h, and then began to increase again. For the cell operating at 170 °C, the resistance overpotential increased gradually from approximately 500 h and then more rapidly after roughly 5000 h, as shown in Fig. 7(b). The loss excluding resistance increased gradually from 500 h, became constant from 2500 to 3000 h, and then increased sharply again after 4000 h. Further, for the cell operating at 190 °C, as shown in Fig. 7(c), the resistance overpotential remained constant from 250 to about 1000 h, after which it sharply increased. The loss excluding resistance increased rapidly from approximately 250 h, became constant after 500 h, and then increased sharply again from 1000 h.

Although the cell voltage deterioration rate varies with temperature, the losses excluding resistance showed a similar trend in all cells: an initial increase, an almost flat period, and finally a sharp increase accompanying the final reduction of cell voltage. Furthermore, the resistance overpotential in the 170 and 190 °C cells also showed a tendency to increase sharply as if synchronized with the final increase of the loss excluding resistance.

Fig. 8 shows TEM images of electrode catalysts, (a) just prior to assembly into the cell (see Section 2.2), (b) after a power generation test at 150 °C for 1029 h, and (c) after a power generation test at 190 °C for 1220 h (see Fig. 4(c)). Particle size distributions and mean particle diameters for the platinum–cobalt grains are also shown in Fig. 8. As seen in Fig. 8(a), the mean particle diameter in the catalyst before power generation was 3.8 nm. However, following power generation for approximately 1000 h at 150 and 190 °C, the mean diameters of the catalyst particles grew to 4.1 and 6.0 nm, respectively, as shown in Fig. 8(b) and (c). In previous studies, it was also reported that the size of platinum catalyst particles grew during power generation in a relatively short period of approximately 500 h at 150 °C [28–31]. Further, Zhai et al. showed that platinum aggregation occurs in the early stage of power generation and that the cell performance is reduced due to a decrease in the specific surface area of the platinum particles and an increase in the reaction resistance [31]. Taking these results into account, it is suggested that grain growth in the catalysts is largely responsible for the reduction of cell voltage of approximately 20 mV in the initial period of the durability test, due to an increase of the activation overpotential. However, since the cell voltage remains constant for a long time after its initial drop of 20 mV, as shown in Fig. 7, it is believed that some other factor is responsible for the final drop in cell voltage and increase of resistance overpotential. In order to investigate factors other than catalyst particle aggregation, OCV, impedance, and SEM surface measurements were carried out.

Fig. 9 shows the time dependence of the OCV drop for the 170 °C cell in the final period from 4700 to 6400 h, together with the data for resistance overpotential and loss excluding resistance, which were already presented in Fig. 7(b). The OCV was found to decrease by approximately 25 mV during this period, while the resistance overpotential increased by approximately 10 mV. If the OCV reduction of 25 mV is subtracted from the loss excluding resistance of 35 mV, then the increased portion of the activation and diffusion overpotential is approximately 10 mV. Thus, it can be concluded that the reduction in the OCV is the dominant factor involved in the cell voltage drop during the terminal period of cell life.

Fig. 10(a) and (b) shows SEM micrographs of the surface of the acid-doped PBI electrolyte membrane before and after power generation for 6400 h at 170 °C, respectively. In Fig. 10(b), some localized holes are seen in the cell membrane. It is thought that, in the final stages of cell life, H_2 crossover via such holes leads to the generation of $HO^{\bullet}$ and $HO_2^{\bullet}$ radicals that accelerate membrane deterioration, resulting in the reduction of OCV. There has been a report regarding such an attack on the electrolyte membrane by $HO^{\bullet}$ and $HO_2^{\bullet}$ radicals [30], and this has been suggested as being the main cause of termination of the cell life. In order to further investigate the cause of such damage to the membrane, impedance

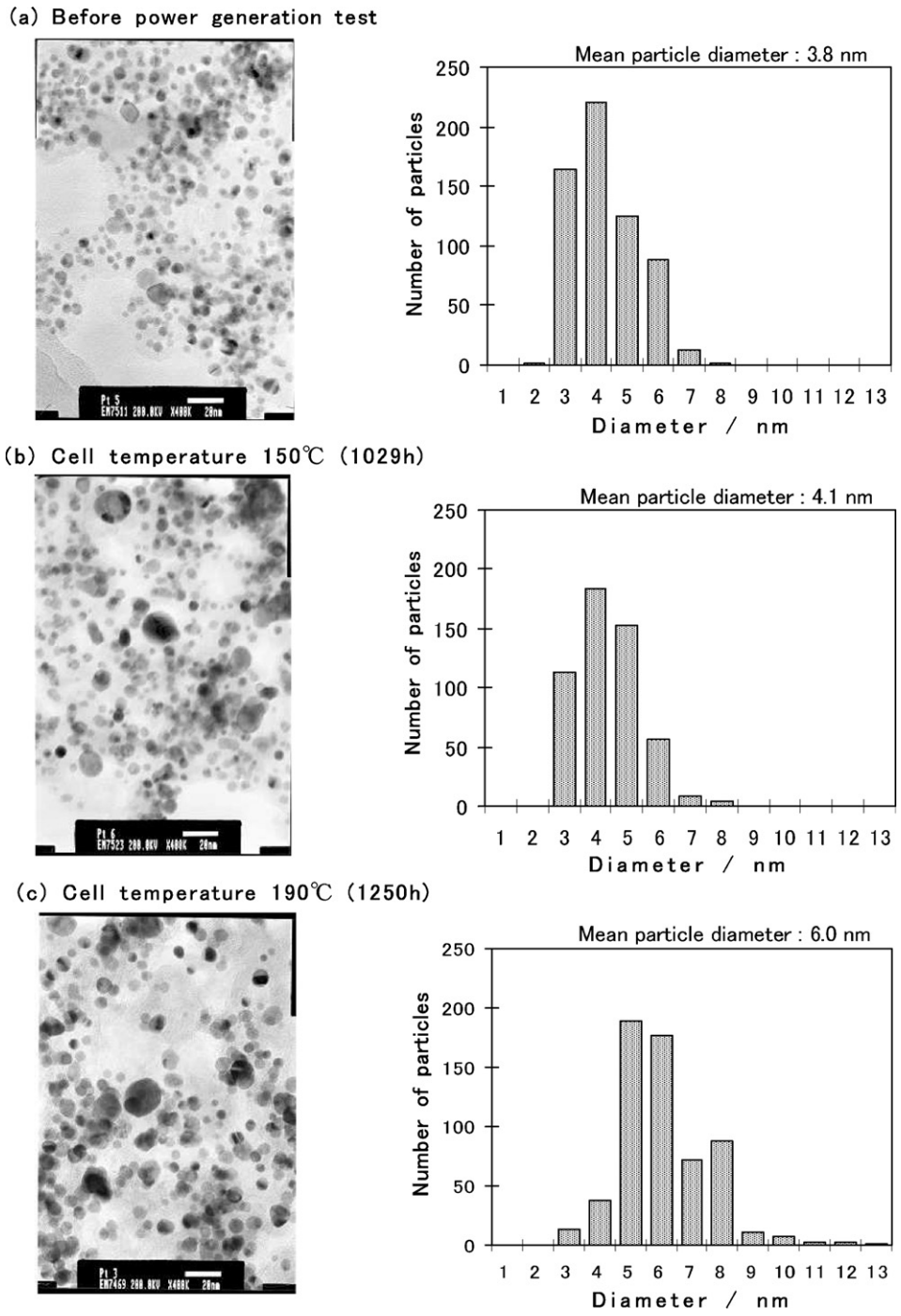

Fig. 8. TEM micrographs of the Pt–Co catalyst (a) before the power generation test, (b) after 1029 h operation at 150 °C, and (c) after 1250 h operation at 190 °C.

measurements were conducted on the 170 °C cell during the terminal period of its life.

Fig. 11 shows Cole–Cole plots of the 170 °C cell obtained by impedance measurements at 5000 h when the cell voltage started to decrease significantly, and at 6400 h when the power generation was terminated. Fig. 12 shows the dependence of ohmic, charge transfer, and mass transport resistance on the operation time, taken from the data of Fig. 11. Both figures show an increase in the ohmic and charge transfer resistance from 5000 to 6400 h. In contrast, the mass transport resistance decreases, even at a low current density of 0.2 A cm^{-2}, as the gas diffusion rate improves. On the other hand, the authors have previously reported that lower phosphoric acid doping, i.e., less phosphoric acid in the catalytic layer, increases both the ohmic and charge transfer resistances, and consequently reduces the cell voltage [36]. On the basis of these results, it is considered likely that the phosphoric acid in the membrane and catalyst layers gradually evaporates and finally dries out during long-term operation, resulting in an increase in both the ohmic and charge transfer resistance, while concurrently enhancing gas diffusion and reducing the diffusion resistance. Although it is as yet unclear whether radical attack on the membrane or the drying up of phosphoric acid acts as the trigger, it is obvious that the latter directly or indirectly determines the cell lifetime.

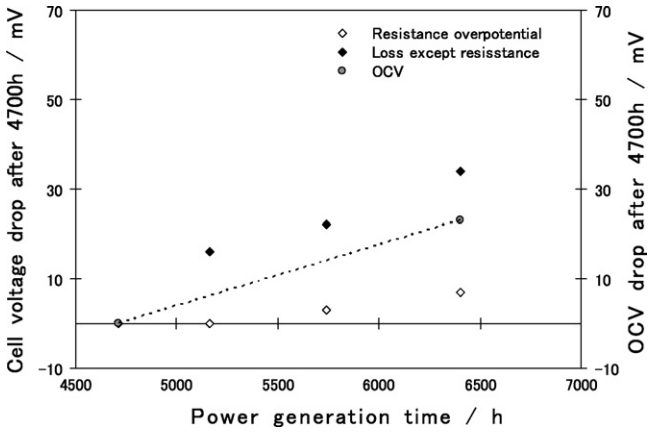

Fig. 9. OCV and cell voltage drop of the cell operated at 170 °C from 4700 h.

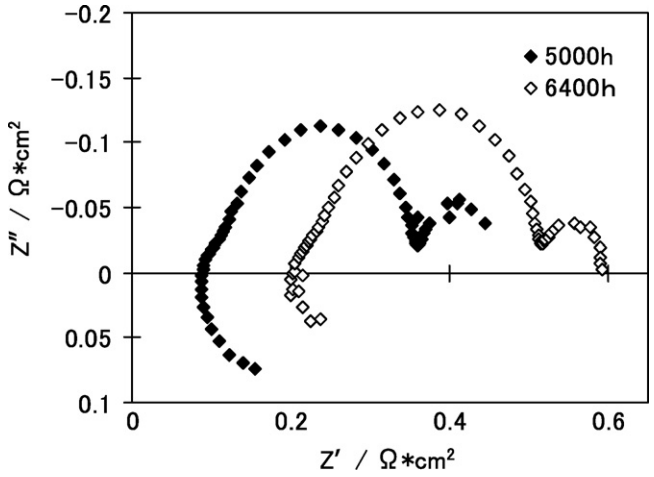

Fig. 11. Cole–Cole plot for the cell operated at 170 °C for 5000 h and after power generation.

The effect of phosphoric acid reduction on cell performance has been investigated also for phosphoric acid-type fuel cells. Fig. 13 shows the results of an evaluation by Okae et al. of the amount of phosphoric acid evaporation as a function of cell temperature in a phosphoric acid fuel cell (PAFC) [39]. The evaporation rates estimated from Fig. 13 are 0.6, 1.8, and 9 $\mu g\,m^{-2}\,s^{-1}$ for cell temperatures of 150, 170, and 190 °C, respectively.

Fig. 14 shows the weight of evaporated acid per unit area as a function of time, calculated from the data of Fig. 13, overlaid with the time dependence of the voltage drop at 0.2 $A\,cm^{-2}$, based on the data of Fig. 4. The cell voltages shown here represent those values that had dropped by 10% from the peak voltage. However, since the cell operating at 150 °C was still generating power, the plotted data corresponds to lower voltage drops. It can be seen that the phosphoric acid depletion rate and the cell voltage reduction rate are in good agreement, regardless of cell temperature. Thus, even though the initial reduction of cell voltage is thought to be caused by the increase in the catalyst particle size, the depletion of phosphoric acid has a substantial effect on the cell voltage over the entire lifetime of the cell. The fact the voltage drop in the 150 °C cell was still less than 7% after 16,000 h operation suggests that the cell remains functioning by use of its remaining volume of phosphoric acid.

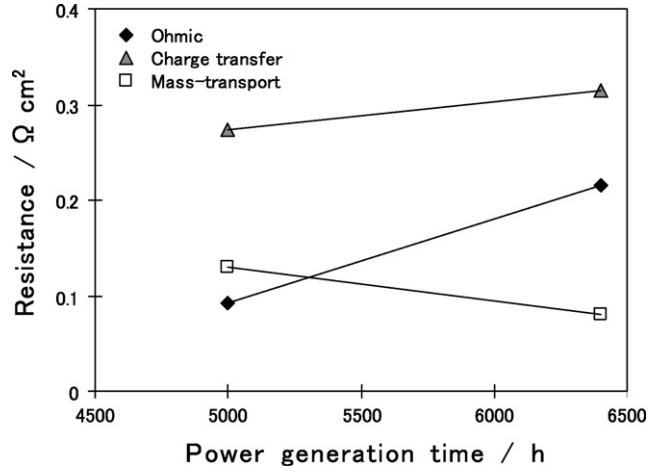

Fig. 12. Time course of ohmic, charge transfer and mass transport resistance in the final stage of lifetime for the cell operated at 170 °C.

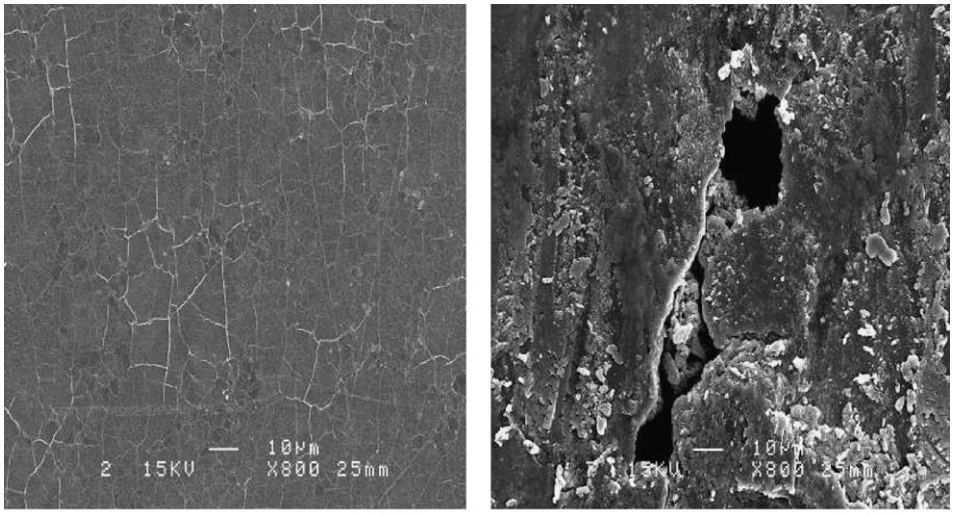

(a) **Membrane after doping**

(b) **Membrane after power generation test at 170°C**

Fig. 10. SEM micrographs of electrolyte membranes after doping and after the power generation test at 170 °C.

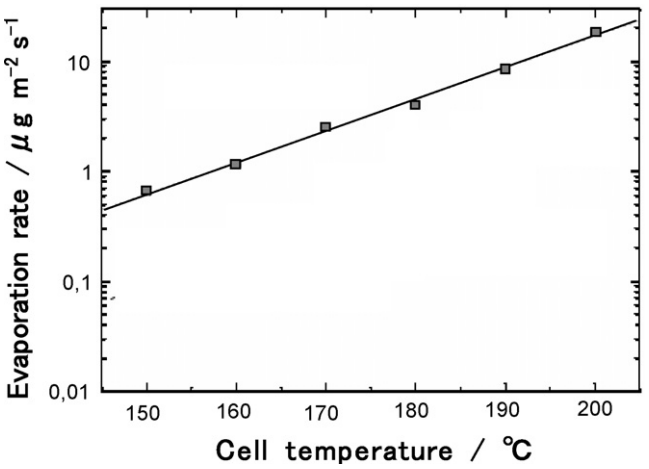

Fig. 13. Phosphoric acid evaporation rate as a function of temperature, from Ref. [43].

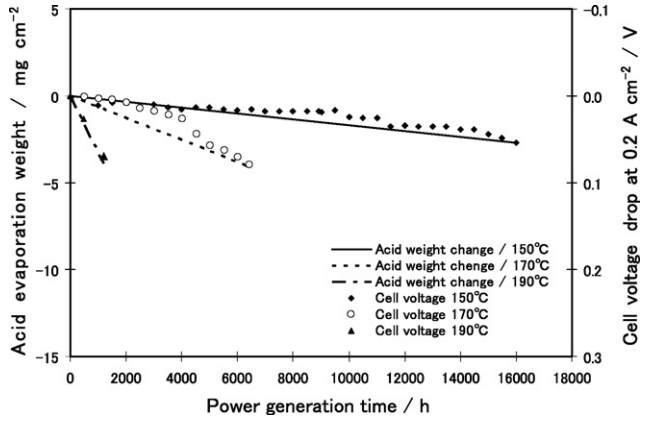

Fig. 14. Relationship between the acid weight change by evaporation and the cell voltage drop. Solid, dotted, dot-dashed lines show the acid weight changes calculated for cell temperatures of 150, 170, and 190 °C, respectively. Solid symbols (♦, ○, ▲) indicate the cell voltage drops at 0.2 cm^{-2}.

4. Conclusion

For HT-PEMFCs using PBI membranes doped with phosphoric acid, the effects of cell temperature on cell performance and durability were evaluated by long-term durability tests at cell temperatures of 150, 170, and 190 °C. Consequently, it was clarified that a higher cell temperature results in a higher cell voltage, but a shorter cell life.

The reduction in cell voltage of approximately 20 mV during the long-term power generation tests was considered to be caused both by aggregation of the electrode catalyst particles in the early stages of operation, in addition to the effects of crossover due to the depletion of phosphoric acid in the terminal stage, the latter regardless of cell temperature. However, the cell operating at 150 °C was still generating power after 16,000 h, and it is expected that enhanced long-term durability for practical applications can be achieved through effective management of phosphoric acid transfer.

References

[1] M. Kawahara, 5th Int'l Hydrogen & Fuel Cell Expo Keynote, 2009, p. 17.
[2] J. Baurmeister, T. Kohno, Proceedings of the 13th Fuel Cell FCDIC Symposium, 2006, p. 122.
[3] P. Krishnan, J.S. Park, C.S. Kim, J. Power Sources 159 (2006) 817.
[4] H. Xu, Y. Song, H.R. Kunz, J.M. Fenton, J. Power Sources 159 (2006) 979.
[5] C.P. Wang, H.S. Chu, Y.Y. Yan, K.L. Hsueh, J. Power Sources 170 (2007) 235.
[6] J. Zhang, Y. Tang, C. Song, J. Zhang, J. Power Sources 172 (2007) 163.
[7] Q. Li, R. He, J.O. Jensen, N.J. Bjerrum, Chem. Mater. 15 (2003) 4896.
[8] M. Kawahara, J. Morita, M. Rikukawa, K. Sanui, N. Ogata, Electrochim. Acta 45 (2000) 3045.
[9] R. He, Q. Li, G. Xiao, N.J. Bjerrum, J. Membr. Sci. 226 (2003) 169.
[10] Q. Li, R. He, J.O. Jensen, N.J. Bjerrum, Fuel Cells Fundam. Syst. 4 (2004) 147.
[11] P. Staiti, F. Lufrano, A.S. Arico, E. Passalacqua, V. Antonucci, J. Membr. Sci. 188 (2001) 71.
[12] P. Staiti, M. Minutoli, J. Power Sources 94 (2001) 9.
[13] R. Bouchet, E. Siebert, Solid State Ionics 118 (1999) 287.
[14] X. Glipa, B. Bonnet, B.B. Mula, D.J. Jones, J. Roziere, J. Mater. Chem. 9 (1999) 3045.
[15] H. Pu, W.H. Meyer, G. Wegner, J. Polym. Sci. B: Polym. Phys. 40 (2002) 663.
[16] B. Xing, O. Savadogo, Electrochem. Commun. 2 (2000) 697.
[17] P. Donoso, W. Gorecki, C. Berthier, F. Defendini, C. Poinsignon, M. Armand, Solid State Ionics 28–30 (1988) 969.
[18] S.P. Weeks, J.J. Zupancic, J.R. Swedo, Solid State Ionics 31 (1988) 117.
[19] M.A. Vargas, R.A. Vargas, B.E. Mellander, Electrochim. Acta 44 (1999) 4227.
[20] J.C. Lassègues, B. Desbat, O. Trinquet, F. Cruege, C. Poinsignon, Solid State Ionics 35 (1989) 17.
[21] D. Rogriguez, C. Jegat, O. Trinquet, J. Grondin, J.C. Lassègues, Solid State Ionics 61 (1993) 195.
[22] M.F. Daniel, B. Desbat, F. Cruege, O. Trinquet, J.C. Lassègues, Solid State Ionics 28–30 (1988) 637.
[23] J.A. Asensio, S. Borros, P.G. Romero, J. Electrochem. Soc. 151 (2004) A304.
[24] Y.L. Ma, J.S. Wainright, M.H. Litt, R.F. Savinell, J. Electrochem. Soc. 151 (2004) A8.
[25] J.R.P. Jayakody, S.H. Chung, L. Durantio, H. Zhang, L. Xiao, B.C. Benicewicz, S.G. Greenbaum, J. Electrochem. Soc. 154 (2007) B242.
[26] N.H. Jalani, M. Ramani, K. Ohlsson, S. Buelte, G. Pacifico, R. Pollard, R. Staudt, R. Datta, J. Power Sources 160 (2006) 1096.
[27] Z. Qi, S. Buelte, J. Power Sources 161 (2006) 1126.
[28] Y. Zhai, H. Zhang, G. Liu, J. Hu, B. Yi, J. Electrochem. Soc. 154 (2007) B72.
[29] J. Hu, H. Zhang, G. Liu, B. Yi, Hydrogen Energy 31 (2006) 1855.
[30] G. Liu, H. Zhang, J. Hu, Y. Zhai, D. Xu, Z. Shao, J. Power Sources 162 (2006) 547.
[31] Y. Zhai, H. Zhang, D. Xing, Z.G. Shao, J. Power Sources 164 (2007) 126.
[32] J. Lobato, P. Canizares, M.A. Rodrigo, J.J. Linares, Electrochim. Acta 52 (2007) 391.
[33] J.H. Kim, H.J. Kim, T.H. Lim, H.I. Lee, J. Power Sources 170 (2007) 275.
[34] C. Pan, Q. Li, J.O. Jensen, R. Je, L.N. Cleemann, M.S. Nilsson, N.J. Bjerrum, Q. Zeng, J. Power Sources 172 (2007) 278.
[35] A. Sounai, K. Sakai, Proceedings of the 13th Fuel Cell FCDIC Symposium, 2006, p. 125.
[36] Y. Oono, A. Sounai, M. Hori, J. Power Sources 189 (2009) 943.
[37] J. Yu, Y. Yoshikawa, T. Matsuura, M.N. Islam, M. Hori, Electrochem. Solid-State Lett. 8 (3) (2005) A152.
[38] J. Yu, T. Matsuura, Y. Yoshikawa, M.N. Islam, M. Hori, Electrochem. Solid-State Lett. 8 (3) (2005) A156.
[39] I. Okae, S. Kato, A. Seya, T. Kamonoshita, The Chemical Society of Japan 67th Spring Meeting, 1990, p. 148.